bioRxiv preprint doi: https://doi.org/10.1101/614040; this version posted June 11, 2019. The copyright holder for this preprint (which was not certified by peer review) is the author/funder, who has granted bioRxiv a license to display the preprint in perpetuity. It is made available under aCC-BY-NC 4.0 International license.

Low Dose Ionizing Radiation Strongly Stimulates Insertional Mutagenesis in a γH2AX Dependent Manner

Alex N. Zelensky[1,2*], Mascha Schoonakker[1], Inger Brandsma[1], Marcel Tijsterman[3], Dik C. van Gent[1,2], Jeroen Essers[1,4,5], Roland Kanaar[1,2*]

[1]Department of Molecular Genetics, [2]Oncode Institute, Erasmus MC, PO Box 2040, 3000 CA, Rotterdam, The Netherlands

[3]Human Genetics, Leiden University Medical Center, PO Box 9600, 2300 RC, Leiden, The Netherlands

[4]Department of Radiation Oncology, Erasmus MC, PO Box 2040, 3000 CA, Rotterdam, The Netherlands

[5]Department of Vascular Surgery, Erasmus MC, PO Box 2040, 3000 CA, Rotterdam, The Netherlands

* Corresponding authors: r.kanaar@erasmusmc.nl and a.zelensky@erasmusmc.nl

bioRxiv preprint doi: https://doi.org/10.1101/614040; this version posted June 11, 2019. The copyright holder for this preprint (which was not certified by peer review) is the author/funder, who has granted bioRxiv a license to display the preprint in perpetuity. It is made available under aCC-BY-NC 4.0 International license.

Abstract

Extrachromosomal DNA can integrate into the genome with no sequence specificity producing an insertional mutation. This process, which is referred to as random integration (RI), requires a double stranded break (DSB) in the genome. Inducing DSBs by various means, including ionizing radiation, increases the frequency of integration. Here we report that non-lethal physiologically relevant doses of ionizing radiation (10-100 mGy), within the range produced by medical imaging equipment, stimulate RI of transfected and viral episomal DNA in human and mouse cells with an extremely high efficiency. Genetic analysis of stimulated RI (S-RI) revealed that it is distinct from the background RI, requires histone H2AX S139 phosphorylation (γH2AX) and is not reduced by DNA polymerase θ (Polq) inactivation. S-RI efficiency was unaffected by the main DSB repair pathway (homologous recombination and non-homologous end joining) disruptions, but double deficiency in MDC1 and 53BP1 phenocopies γH2AX inactivation. The robust responsiveness of S-RI to physiological amounts of DSBs has implications for radiation risk assessment and can be exploited for extremely sensitive, macroscopic and direct detection of DSB-induced mutations.

Keywords:
Random integration, extrachromosomal DNA, insertional mutagenesis, γH2AX, DSB repair, low dose irradiation.

bioRxiv preprint doi: https://doi.org/10.1101/614040; this version posted June 11, 2019. The copyright holder for this preprint (which was not certified by peer review) is the author/funder, who has granted bioRxiv a license to display the preprint in perpetuity. It is made available under aCC-BY-NC 4.0 International license.

Introduction

Extrachromosomal DNA – endogenous, viral or transfected – can integrate into the genomic DNA, resulting in an insertional mutation. This type of mutagenesis has been primarily studied in the context of exogenous DNA that enters the nucleus as a result of transfection or viral infection, and has several important practical implications [1]. It is used to produce transgenic cell lines and organisms for research and biotechnological applications. Random integration (RI) of transcription-blocking constructs has been exploited as a form of untargeted but traceable mutagenesis ("gene trapping"). Integration of exogenous DNA is an important factor in several therapeutic approaches, where it is regarded as beneficial (stable restoration of a missing gene) or dangerous (insertion near an oncogene and its activation). Viral integration into the genome has been considered as a contributing factor in oncogenesis, even for viruses that do not encode an active integration function [2]. During precise homology-driven modification of the genome (gene targeting), random integration of the targeting construct is an unwanted side effect that severely limits the application of this powerful technique in the vast majority of organisms [3].

The presence of extrachromosomal DNA is a physiological condition, as a sizable pool of it exists in the majority of normal cells in tissues, and includes fragments of nuclear and mitochondrial DNA released due to damage repair, telomeric DNA circles [4], non-integrating viral genomes [5], mobile genetic elements and phagocytized extracellular DNA [6]. According to one estimate, the relative fraction of such extrachromosomal DNA in normal tissues can be substantial, reaching 0.1-0.2% of total DNA content [7], which is comparable to other major genomic components such as telomeres (0.4%). How episomal DNA interacts with the genomic DNA and repair systems is not well understood.

Insertion of exogenous DNA into a chromosome can be described by a simple and intuitive model as mis-repair of a double strand break (DSB) in the genomic DNA by non-homologous end joining that traps an extrachromosomal DNA fragment happening to be in the vicinity of the DSB [8,9]. This model predicts that the proximity of an ongoing DSB repair event to an extrachromosomal DNA molecule will determine the frequency of the insertion, and therefore that increasing the frequency of DSBs above background by inflicting additional damage will increase the likelihood of integration. This prediction has been confirmed numerous times in various cell lines and with different DNA vectors using doses of > 0.5 Gy of ionizing radiation (γ- and X-rays), which is arguably the best-studied method of DSB induction [10-23]. RI stimulation by DSB-inducing chemicals and enzymes has also been demonstrated, as well as some non-DSB inducing genotoxic agents. [16,21,24-35] In the latter case the stimulation can be explained by indirect DSB induction during replication.

Genomic integration of extrachromosomal DNA is referred to in the existing literature as RI, illegitimate recombination, illegitimate integration, stable integration, stable transformation, non-homologous integration or insertional mutation [8]. Although it is not perfect, we chose to use the

bioRxiv preprint doi: https://doi.org/10.1101/614040; this version posted June 11, 2019. The copyright holder for this preprint (which was not certified by peer review) is the author/funder, who has granted bioRxiv a license to display the preprint in perpetuity. It is made available under aCC-BY-NC 4.0 International license.

first term. In the context of RI stimulated by DNA lesions we use the term stimulated RI (S-RI). Here we report the following, and to our knowledge so far unidentified, properties of the S-RI phenomenon. Firstly, we found that extremely low doses (10-50 mGy), similar to those encountered during routine medical diagnostic procedures, strongly stimulate the integration of transfected DNA and episomal viral DNA. Secondly, a screen of multiple knock-out mouse embryonic stem (ES) cell lines revealed that contrary to expectation, disruption of the two major DSB repair pathways has no effect on S-RI, and thirdly we showed that phosphorylation of H2AX on serine 139 and recruitment of the adaptor protein MDC1, involved in DNA damage response, are essential for the process.

Results

Integration is strongly stimulated by physiologically relevant doses of radiation

To investigate the effect of low dose irradiation (< 1 Gy) on RI we transfected ES cells by electroporation with circular or linearized plasmid DNA containing a puromycin resistance gene, divided the cells equally over several culture dishes, and irradiated the dishes using ^{137}Cs γ-irradiation source with a set of doses ranging from 0.01 to 1 Gy **[Fig 1A,B]**. Remarkably, even the lowest dose tested already led to an increase in the number of puromycin-resistant colonies formed after 6-8 days of selection **[Fig 1B]**, with a 7.5±0.8 -fold increase at a dose of 200 mGy. The response was linear between 10 and 200 mGy, then plateaued between 200 and 500 mGy, and decreased at 1 Gy.

The sensitivity of the response to the extremely low doses, the plateauing dose response, and the high magnitude of the stimulation (up to 10-fold) distinguish our findings from numerous previous reports of the phenomenon, as they generally studied doses above 1 Gy [12-19,22]. It is remarkable that the exquisite sensitivity of the assay to physiologically relevant amounts of induced DNA damage appears to have escaped experimental scrutiny for more than half a century. Intrigued by this, we went on to verify the generality of the S-RI phenomenon using different DSB induction methods, cell lines, DNA vectors and assay endpoints. The lower end of the dose range we tested overlaps the dose range of certain medical imaging procedures (e.g. 1-30 mGy for computed tomography (CT) and fluoroscopy [24]). We scanned freshly transfected ES cell suspension in a micro-CT instrument (Quantum FX, PerkinElmer) used for mouse imaging. One to five sequential scans were performed at the lowest resolution, each scan delivering 13 mGy based on the manufacturer's data. A single scan produced a clear increase in integration frequency (2.28 ±0.17, n=7) and consecutive scans resulted in a dose response curve similar to what we observed with the ^{137}Cs source **[Fig 1C]**. Human HeLa cells transfected with the plasmid DNA by electroporation or lipofection performed similarly to mES cells in the S-RI colony formation assay **[Fig S1A,B]**.

To confirm that our observations were not limited to plasmid DNA transfection or antibiotic selection, we performed S-RI experiments using non-replicating episomal viral vectors and with fluorescent marker detection by FACS. Recombinant adeno-associated virus type 2 (rAAV2) has a single-stranded

bioRxiv preprint doi: https://doi.org/10.1101/614040; this version posted June 11, 2019. The copyright holder for this preprint (which was not certified by peer review) is the author/funder, who has granted bioRxiv a license to display the preprint in perpetuity. It is made available under aCC-BY-NC 4.0 International license.

DNA genome, and while it can integrate in cultured human cells with some sequence specificity conferred by the *rep* protein, wild-type AAV2 infecting human tissues and *rep*-deleted rAAV2 vectors persist as episomes and integrate infrequently and with no detectable specificity [5,25]. We added lysates containing rAAV2 particles encoding GFP to the HeLa cell culture media, incubated overnight to allow infection to occur, re-seeded the cells into a series of dishes and irradiated them with 0.02-1 Gy. The fraction of cells expressing GFP was ~60% two days after the infection and gradually decreased over time due to dilution and loss of rAAV2-GFP episomes in dividing cells. At day 13 only 0.05-0.1% of unirradiated cells remained GFP-positive, presumably due to stable integration [26]. The GFP-positive fraction increased linearly with the dose in irradiated cells **[Fig 1D, S1C]**. Transfection of human U2OS cells with plasmid DNA containing a GFP minigene, followed by FACS 14-21 days later, further confirmed that selection is not required to observe the S-RI effect **[Fig S1D]**. We also observed S-RI **[Fig 1E]** with integrase-deficient HIV-1 lentiviral (IDLV) vectors [27,28] whose RNA genomes are reverse-transcribed normally, but accumulate as circular or linear episomal DNA because of the inactivating D64V mutation in the integrase [29].

Both IDLV and rAAV vectors were used previously to detect nuclease-induced DSBs [26,30,31]. To show that transfected plasmid DNA also integrates at the DSBs we used the DiVA-AID cell line, which allows precise control over nuclear localization and degradation of the AsiSI nuclease that has hundreds of recognition sites in human genome [32]. We added 4-hydroxytamoxifen to induce AsiSI breaks immediately after the transfection of plasmid DNA, and controlled the DSB dose by inducing AsiSI degradation by adding auxin to the media 1 or 4 hours later **[Fig 1F]**. The dose-dependent increase in the number of colonies we observed was consistent with the results we obtained using ionizing radiation.

To better characterize the parameters affecting S-RI we studied its dependence on the timing of irradiation and on the amount of transfected DNA. The stimulatory effect of irradiation dropped precipitously shortly after transfection, but was still observed as late as 24 hours later when circular plasmid DNA was used **[Fig S1E,F]**. We also performed an experiment in which the order of transfection and irradiation was reversed, and still observed a stimulatory effect **[Fig S1G]**. This demonstrates that S-RI is caused by the effect of IR on the host cell rather than on the transfected DNA, further supporting the notion that the stimulation is achieved by DSB induction in the genomic DNA. By modifying the amount of DNA electroporated into mES cells we revealed a striking and opposing effects on S-RI and background RI **[Fig 1G, S1H,I]**. When DNA amounts were low (2 µg), S-RI was very efficient, and background RI was low, while when high amount of DNA was electroporated (100 µg), S-RI became inefficient, and background RI increased.

S-RI requires γH2AX but not HR or NHEJ

A simple explanation to S-RI is that radiation creates DSBs into which transfected DNA can be ligated. This model predicts that cells in which major DSB repair mechanisms, such as homologous

bioRxiv preprint doi: https://doi.org/10.1101/614040; this version posted June 11, 2019. The copyright holder for this preprint (which was not certified by peer review) is the author/funder, who has granted bioRxiv a license to display the preprint in perpetuity. It is made available under aCC-BY-NC 4.0 International license.

recombination (HR) and non-homologous end joining (NHEJ), are disrupted, will be more responsive to S-RI, unless the repair deficiency negatively affects the enzymes involved in integration itself. We performed the S-RI assay in mES cell lines where key DNA damage repair and response genes were genetically inactivated. Surprisingly, we observed wild-type dose response curves in *Rad54*$^{-/-}$ ES cells, which have an HR deficiency phenotype [33], and in *p53*$^{-/-}$ cells lacking key DNA damage signaling mediator, while in *DNA-PKcs*$^{-/-}$ (*Prkdc*$^{-/-}$) cells deficient in a canonical NHEJ enzyme [34] a small reduction in S-RI was observed **[Fig 2A]**. We recently demonstrated that in mES cells DNA polymerase θ is responsible for the majority of background RI [35], and canonical NHEJ proteins Ku70, Ku80 and LigIV become important in the absence of Pol θ; and similar observations were reported in human cells [36]. Surprisingly, S-RI was increased rather than suppressed in the Pol θ-deficient cells (*Polq*$^{-/-}$), and in the Ku mutants **[Fig 2B]**, which suggests that S-RI and background RI have distinct genetic dependencies.

In sharp contrast, cells deficient for H2AX [37,38], a histone variant whose post-translational modifications are central to DNA damage response signaling, were near-completely immune to RI stimulation by irradiation **[Fig 2A]**. This was difficult to reconcile with the previously described phenotypes of *H2ax*$^{-/-}$ cells, which are prone to translocations [39,40] suggesting increased frequency of DSBs in the absence of a major NHEJ defect. Background RI was normal in *H2ax*$^{-/-}$ lines **[Fig S2A]**, further indicating that RI and S-RI are genetically distinct processes.

The S-RI defect was observed in two different *H2ax*$^{-/-}$ cell lines and could be reverted by inserting a wild-type copy of *H2ax* into the *Rosa26* "safe harbor" locus **[Fig 2C, S2B,C]**. We also tested variants of H2AX with mutations in residues that are phosphorylated (S139) or ubiquitinated (K13, K15, K118, K119) during DNA damage response signaling [41-43], as well as Y142 required for interaction with the key downstream effector MDC1 [44]. Mutations in the lysines – these residues are common to all H2A variants – did not impair S-RI, while S139A and Y142A mutants were indistinguishable from uncomplemented *H2ax*$^{-/-}$ cells **[Fig 2C]**.

To determine if S-RI was permanently blocked or just stunted by *H2ax* inactivation we performed a broad-dose S-RI experiment **[Fig 2D, S2D]**, using doses up to 3 Gy. The gradual increase in S-RI efficiency we observed in *H2ax*$^{-/-}$ cells in this dose range indicated that the end joining reaction responsible for the ligation of extrachromosomal DNA into the IR-induced DSB was inherently functional, but less efficient in the absence of H2AX. H2ax$^{-/-}$ cells were also deficient for RI stimulation by etoposide **[Fig 2E]**, one of DNA topoisomerase II inhibitors, which were previously shown to be potent RI stimulators [45-47].

Finally, we wondered, which of the checkpoint kinases [48] phosphorylating H2AX at the sites of DNA damage is involved in S-RI. Therefore, we performed experiments in the presence of chemical inhibitors: KU-55933 specific for ATM [49], VE-821 specific for ATR [50], wortmannin that has highest specificity for DNA-PKcs [51], and UCN-01 for Chk1 [52] at the concentrations we previously found to be effective in mouse ES cells [53]. We also tested the effect of caffeine, which is widely used as a

bioRxiv preprint doi: https://doi.org/10.1101/614040; this version posted June 11, 2019. The copyright holder for this preprint (which was not certified by peer review) is the author/funder, who has granted bioRxiv a license to display the preprint in perpetuity. It is made available under aCC-BY-NC 4.0 International license.

broadly specific ATM/ATR/DNA-PKcs inhibitor, but which we found to lack this activity in ES cells, and to strongly suppress gene targeting by HR [53-55]. Inhibition of ATM and ATR reduced S-RI efficiency **[Fig S2E]**, and the combination of the two inhibitors had an additive effect, which was even more pronounced in *DnaPKcs*$^{-/-}$ cells **[Fig S2E]**. In contrast UCN-01, caffeine and wortmannin had no effect on S-RI. Taken together these results indicate that S-RI is dependent on phosphorylation of H2AX by one of the partially redundant DNA damage response kinases.

Role of γH2AX-Binding Proteins

Three proteins have been shown to directly bind H2AX in phospho-S139 dependent manner: MDC1 [44], 53BP1 [56] and MCPH1 [57]. We engineered a series of mES knock-out cell lines **[Fig 3, S3-S5]** to test if S-RI deficiency in cells that cannot form γH2AX is due to the failed recruitment of these proteins. Based on its role in promoting DSB repair via NHEJ over HR, 53BP1 would be a good candidate for the role of the downstream effector, however neither the knock-out nor shRNA knock-down of 53BP1 affected S-RI or background RI **[Fig 3A, S3A,B, S4]**. The most pronounced phenotype of MDC1-deficient cells was a significant reduction in background RI, similar in magnitude to what we reported previously for Pol θ [35]. However, unlike in Pol θ-deficient cells **[Fig 2B]**, S-RI was partially suppressed in *Mdc1*$^{-/-}$ cells **[Fig 3A]**, and reduced even further in the double *Mdc1*$^{-/-}$*53bp1*$^{-/-}$ knock-out line. Inactivation of *Mdc1* in *H2ax*$^{-/-}$ cells did not further suppress S-RI, consistent with the downstream role of MDC1 in γH2AX signaling. *Mcph1* knock-out cells behaved like wild-type in the S-RI assay, but had elevated background RI. The *Mcph1* mutation also reverted the partial suppression of S-RI by *Mdc1* inactivation, as *Mdc1*$^{-/-}$*Mcph1*$^{-/-}$ double mutant showed the same S-RI efficiency as wild-type cells. Since we established that MDC1 contributes to both RI and S-RI efficiency, the positive effect of MCPH1 deletion can be explained by its competition with MDC1 for phospho-S139 binding.

Discussion

We used a simple assay to re-examine a phenomenon known since the early days of research on cultured eukaryotic cells [22,23]. This makes a number of unexpected observations regarding radiation-stimulated integration of extrachromosomal DNA we present here all the more interesting. The most important of them are: high sensitivity to very low, physiologically relevant doses of irradiation, non-linear dose dependence, independence of the best known DSB repair pathways, NHEJ and HR, requirement of γH2AX for stimulated but not background RI, and the complex involvement of γH2AX-interacting proteins.

Despite numerous reports describing the stimulation of RI by ionizing radiation, to our knowledge our study for the first time reports the effects of doses <0.5 Gy, and in particular the striking dose-dependent stimulation in the range 0.01-0.2 Gy. Previous studies performed with a dose range of 1-10 Gy with different vertebrate cell lines, vectors and transfection methods, observed linear dose dependence of stable colony numbers after adjustment for IR-induced reduction in survival

bioRxiv preprint doi: https://doi.org/10.1101/614040; this version posted June 11, 2019. The copyright holder for this preprint (which was not certified by peer review) is the author/funder, who has granted bioRxiv a license to display the preprint in perpetuity. It is made available under aCC-BY-NC 4.0 International license.

[12,15,18,19,22,23]. Explanation of the dose-response curve plateauing we observed in the majority of experimental systems we used **[Fig 1, S1]**, and seen in some previous studies [14,17], requires a model that considers more than just chromosomal DSBs as the factor limiting extrachromosomal DNA integration. What can be the other bottleneck(s)? Transfection efficiency is clearly not one, as the frequency of stable integration events (10^{-2}-10^{-4}) is orders of magnitude lower than the number of transfected cells (>10^{-1}). Furthermore, we observed that decreasing the amount of transfected DNA makes S-RI *more* efficient. The nature of the barrier limiting S-RI, which may be cell-intrinsic (e.g. capacity of a DNA-binding protein, signals triggered by DSBs or transfected DNA above a certain threshold), or reflect heterogeneity in the cell population, remains to be determined.

γH2AX as a central factor involved in stimulated random integration

We observed a striking and unanticipated difference in S-RI between the wild-type and the *H2ax*$^{-/-}$ ES cells. Although γH2AX is a widely used DNA damage marker and actively studied as such [reviewed by 58], the effects of H2AX deficiency on cells and organisms are generally described as "moderate" or "mild" [37,38,59-62], and **[Fig S2D]**. The near-absolute dependence of S-RI on γH2AX is among the most striking H2AX phenotypes discovered to date. Several ways a DNA repair protein may affect RI can be envisaged: by direct involvement in the NHEJ reaction, indirectly by influencing DSB repair pathway choice or facilitating NHEJ protein recruitment etc., or by changing DSB persistence (longer half-lives due to inefficient repair will increase the probability of encounter between a genomic DSB and an extrachromosomal DNA molecule). Other indirect effects through chromatin mobility or packing (accessibility) can also be considered.

H2AX contributes to efficient repair of DSBs by NHEJ. H2AX-deficient cells have increased frequency of both background and induced chromosomal aberrations [37,38,61]. V(D)J recombination although superficially normal in *H2ax*$^{-/-}$ mice [37,38] has hidden alterations revealed by additional inactivation of p53, Artemis or XLF [58]. On the other hand, sensitivity of H2AX-deficient cells to ionizing radiation ranges from moderate [37] to marginally detectable [61], and is always lower than core NHEJ mutants [37]. Moreover, some of this increased sensitivity can be attributed to impaired HR [38,61,63,64] and a compromised G2/M DNA damage checkpoint [61,65]. Assays monitoring mutagenic repair of nuclease-induced DSBs in a chromosomal reporter revealed no effect of H2AX deletion [66]. Data on DSB clearance kinetics in H2AX-deficient cells is conflicting (refs [38,59] vs [67]). Thus, previously described involvement of H2AX in NHEJ does not provide a compelling explanation to S-RI suppression.

Among γH2AX-binding proteins 53BP1 was a prime candidate for the role of the γH2AX-dependent S-RI mediator [68,69], as its retention at DSBs is γH2AX-dependent [62], it promotes DSB repair by NHEJ over HR [70], facilitates of the synapsis between distal DSBs [71] and increases the mobility of a chromosomal DSBs [72]. However, we could only observe the effect of 53BP1 deletion on S-RI when MDC1 was also absent. Moreover, we found that MDC1 rather than 53BP1 contributes to background

bioRxiv preprint doi: https://doi.org/10.1101/614040; this version posted June 11, 2019. The copyright holder for this preprint (which was not certified by peer review) is the author/funder, who has granted bioRxiv a license to display the preprint in perpetuity. It is made available under aCC-BY-NC 4.0 International license.

RI, which was also observed previously in human cells [44,73], and deletion of 53BP1 had no significant effect even when combined with *Mdc1* inactivation. While several studies showed that 53BP1 recruitment to ionizing radiation-induced foci is controlled by MDC1 [74-76], our results suggest an MDC1-indepenent role of 53BP1, as double mutation *Mdc1*$^{-/-}$*53bp1*$^{-/-}$ is required to recapitulate the effect of H2AX deficiency on S-RI.

Are S-RI and RI distinct processes?

The S-RI and background RI have distinct genetic dependencies: while γH2AX is required for S-RI, its loss does not affect background RI; Pol θ has an opposite effect: it is responsible for the majority of background RI events, but its deletion does not impair S-RI; Inactivation of *Mdc1* severely impairs background RI [44,73], but has a much smaller effect on S-RI; *Mcph1* knock-out increases RI efficiency, but has no effect on S-RI unless *Mdc1* is also inactivated. These observations can be interpreted as an indication that S-RI and RI are mechanistically different. However, the models based on this supposition and accommodating the observation we present here and previously [35] are inevitably complex **[Fig S3C]**, and require some uncomfortable assumptions. For example, we found that two out of three γH2AX-binding proteins we studied affect background RI (MDC1 stimulates, MCPH1 suppresses **[Fig S3B]**). If we postulate that background RI itself is γH2AX-independent, we need to conclude that each of the two proteins is coincidentally recruited in some γH2AX-independent manner.

The alternative is to suppose that at least some of the apparent genetic distinctions between RI and S-RI are misleading, or that they stem from the factors that are beyond the simple "[DSB] • [ecDNA] → end joining → insertion" model. As an example of the former, the concentration of background DSBs in the *H2ax*$^{-/-}$ cells (known to be genetically unstable), could be so high as to reach the saturation state that is responsible for the plateauing of the dose-response curve. However, our broad-dose experiment argues against this explanation **[Fig 2D]**. Factors outside of the DSB repair paradigm may include alteration of the cellular state due to DNA damage and antiviral defense checkpoint inductions we alluded to in the discussion of the dose-response plateau, role of H2AX and its interactors in transport, chromatinization, persistence and integrity of the ecDNA, etc. Further genetic exploration of the RI and S-RI phenomena should provide important clues. It is particularly interesting to trace the connection between the upstream signaling proteins (H2AX, MDC1) and the end-joining proteins responsible for the insertion reaction (Pol θ and canonical NHEJ).

Implications

Our results have several important implications. If the robust stimulation of insertional mutagenesis by the doses well below what is currently considered harmful is not limited to cultured cells, it will be important to consider elevated episomal DNA concentration – for example from viral infection – as a confounding factor in assessing the risks of low dose irradiation. The S-RI assay is macroscopic and

bioRxiv preprint doi: https://doi.org/10.1101/614040; this version posted June 11, 2019. The copyright holder for this preprint (which was not certified by peer review) is the author/funder, who has granted bioRxiv a license to display the preprint in perpetuity. It is made available under aCC-BY-NC 4.0 International license.

thus simpler than direct and surrogate mutagenesis assays and damage detection methods (DNA damage response foci counting), and is as sensitive as the alternatives. A high throughput version of it can be developed for determining chemical genotoxicity at physiologically relevant concentrations. It should be stressed that the assay detects irreversible mutagenic events rather than damage that may or may not be repaired.

Analysis of the genetic dependencies of S-RI revealed several unexpected findings, and demonstrated that it provides tools to study functional interactions between the components of the convoluted γH2AX signaling pathway, NHEJ and other DSB repair proteins.

Methods

Cell lines

IB10 mouse ES cells, a clonal isolate of the E14 line [77], and other mouse ES cell lines used in the study were maintained on gelatinized plastic dishes as described [53]. ES cells were grown in 1:1 mixture of DMEM (Lonza BioWhittaker Cat. BE12-604F/U1, with Ultraglutamine 1, 4.5 g/l Glucose) and BRL-conditioned DMEM, supplemented with 1000 U/ml leukemia inhibitory factor, 10% FCS, 1x NEAA, 200 U/ml penicillin, 200 µg/ml streptomycin, 89 µM β-mercaptoethanol. *H2ax*$^{-/-}$ (A) and (N) ES cells were kindly provided by the Alt and Nussenzweig laboratories, respectively [37,38]. HeLa and U2OS cells were grown in DMEM, 10% FCS, 200 U/ml penicillin, 200 µg/ml streptomycin. AID-AsiSI-ER U2OS cells were a king gift of Gaëlle Legube [32]. HEK293T cells were grown in DMEM, 5% FCS, 200 U/ml penicillin, 200 µg/ml streptomycin.

Generation of knock-out ES cell lines with CRISPR/Cas9

Mdc1, *Mcph1,53bp1* knock-out ES cells were produced by CRISPR/Cas9 stimulated gene targeting with plasmid donor **[Fig S4-S5]**. The CRISPR/Cas9 expression plasmid (derived from pX459 [78]) contained one or two sgRNA expression cassettes. Target sequences were (PAM underlined): for *Mdc1* #2 AAGGTAGAGGGGGAAATCTGAGG and #3 AACAGTAGTTCCAGAAAGGTGGG within exons 3 and 4; for *53bp1* #1 TAGTTGAGGTCGGCTTGAGGTGG upstream of the promoter and #2 CCATCAGTCAGGTCATTGAACGG within exon 4; for *Mcph1* promoter targeting #1 CCGGCGCTTAAGGCGACGAAAGG and #2 AAAGCAACTTGAGGATATGGGGG, for *Mcph1* exon 4-5 #3 TGTTCATCGGTATTCACTGCAGG and #4 TGTGCCTGACAGCTACAGGGAGG. Donor constructs contained PGK-hyrgo (*Mdc1*) or PGK-neo (*Mcph1, 53bp1*) selection cassettes. *Mdc1*$^{-/-}$*53bp1*$^{-/-}$ and *Mdc1*$^{-/-}$*Mcph1*$^{-/-}$ cells were produced from the *Mdc1*$^{-/-}$ cell line. For each genotype two to four independent clones were used in experiments.

For H2ax complementation NotI-linearized *Rosa26* [79] targeting vectors containing the human H2AX CDS under the *H2ax* promoter and with *H2ax* 3'UTR were electroporated into ~1-2×10^7 *H2ax*$^{-/-}$(N) ES cells. The vectors were derived from *Rosa26* gene targeting vector pHA416 (a kind gift from Hein te

bioRxiv preprint doi: https://doi.org/10.1101/614040; this version posted June 11, 2019. The copyright holder for this preprint (which was not certified by peer review) is the author/funder, who has granted bioRxiv a license to display the preprint in perpetuity. It is made available under aCC-BY-NC 4.0 International license.

Riele) containing *Salmonella typhimurium* hisD coding sequence. Two days after electroporation selection with 2 or 4 mM L-hisitidinol (Sigma, H6647) was started. Media was replaced every 2-4 days for 10-14 days; colonies were picked and expanded. Single copy integration into the *Rosa26* locus was confirmed by DNA hybridization on BamHI-digested genomic DNA with a 5' probe (PstI-SalI fragment, from pHA607 [80]). H2AX expression was verified by immunoblotting with anti-γH2AX (Millipore mouse mAb clone JBW301) or anti-total H2AX antibody (Cell Signaling rabbit polyclonal #2595).

Constructs

Constructs used in this study were generated by homology-based cloning methods: SLIC [81], In-Fusion (Clontech), isothermal Gibson assembly [82] or recombineering with mobile reagents [83]. Pfx50 polymerase (Invitrogen) was used for PCR amplification of the construction elements in most cases, Phusion (Finnzymes) or Platinum Taq (Invitrogen) polymerase were used to amplify from genomic DNA or cDNA. Constructs were partially sequenced to verify the ligation junctions and ensure the absence of PCR-induced mutations. Maps and details are available upon request. List of oligonucleotides and constructs is provided in Supplementary data file 1.

pLPL, the construct used in the majority of S-RI experiments, was derived from the construct loxP-PGK-gb2-neo-polyA-loxP cassette in pGEM-T Easy originally designed to engineer knock-out alleles using recombineering (Francis Stewart lab, distributed at 2007 EuTRACC workshop on recombineering), referred to as pLNL. A dual (bacterial (gb2) and eukaryotic (PGK)) promoter drives the antibiotic resistance gene allowing selection in both hosts. Neomycin phosphotransferase (*neo*) was replaced with puromycin N-acetyltransferase (*pac*, puro) or hygromycin phosphotransferase (hygro) using recombineering to produce pLPL and pLHL, respectively. For linearization pLPL was digested with DraI, phenol-extracted, precipitated with isopropanol and dissolved in deionized water.

H2ax complementation constructs used to insert a single copy of the human or mouse *H2AX* CDS under native mouse *H2ax* promoter and 3'UTR were engineered by replacing the backbone and removing the PGK-polyA cassette from the pHA416 vector (a gift from Hein te Riele) to create a unique XhoI site between the histidinol trap cassette and the 3' homology arm (pAZ025). A 1721-bp fragment of the mouse *H2ax* locus was PCR-amplified using H2AXwhole-F/-R primers first into a shuttle vector, and then re-cloned into pAZ025, resulting in pAZ026. Analogous constructs were engineered with human H2AX and its mutants by PCR amplification of the promoter and UTR regions from pAZ026 and coding sequences from the corresponding pMSCVpuro constructs [43] (pAZ080-pAZ085); Y142A mutation was added by site-directed mutagenesis (pAZ122).

S-RI assays

Drug resistant colony formation was used as a measure of stable RI frequency in the majority of experiments. In a typical experiment 6×10^6 mouse ES cells were electroporated in 450 µl growth media with 10 µg circular or linearized pLPL (puro) or pAZ095 (GFP, puro) plasmid DNA using

bioRxiv preprint doi: https://doi.org/10.1101/614040; this version posted June 11, 2019. The copyright holder for this preprint (which was not certified by peer review) is the author/funder, who has granted bioRxiv a license to display the preprint in perpetuity. It is made available under aCC-BY-NC 4.0 International license.

GenePulser Xcell apparatus (118 V, 1200 µF, ∞ Ω, exponential decay). pEGFP-N1 plasmid (10 µg) was co-electroporated with pLPL to estimate transfection efficiency in the experiments, where absolute targeting efficiency was determined. In the initial experiments electroporated cells were re-suspended in 37-68 ml growth media; the suspension was distributed over 5-8 10 cm dishes at 7 ml per dish. In later experiments, involving larger number of cell lines, electroporated cells were re-suspended in media and equally distributed into 1.5 ml microcentrifuge or 0.2 ml PCR tubes at 0.1-1 ml per tube. Cells were irradiated within 1 hr after seeding with different doses using ^{137}Cs source (Gammacell) or X-ray apparatus (RS320, Xstrahl). A metal attenuator reducing the dose rate by ~50% was used to deliver doses <100 mGy in low-dose irradiation experiments with Cs source. For micro-CT irradiation cells in 6 cm culture dishes or in 1.5 ml microcentrifuge tubes were scanned (Quantum FX, Perkin Elmer) in the low resolution mode (73 mm f.o.v., 17 sec, 148 mm pixel size), repeatedly 1-5 times. The initial number of cells used for electroporation was increased to compensate for low plating efficiency of some knock-out cell-lines (e.g. *H2ax*$^{-/-}$ and their derivatives). After irradiation in microtubes cells were plated in 10 ml media in 10 cm dishes. To estimate plating efficiency at various irradiation doses 2-4 µl aliquots of irradiated cell suspension was plated into 6-well plates in triplicates. Puromycin (1.5 µg/ml) selection was started one day after electroporation; media was changed as required until macroscopically visible colonies were formed. Colonies were washed with PBS, stained with Coomassie Brilliant Blue (100 mg/l in 40% methanol, 10% acetic acid), and counted directly or after photographing. Colony counts were adjusted for transfection and plating efficiencies. RI stimulation was determined by dividing the adjusted number of colonies in irradiated plate by the adjusted number of colonies in unirradiated control. For plotting, averaged data from biological replicates and was fitted with a sigmoid curve using the "[Agonist] vs. response" function in GraphPad Prism software v8. Statistically significant differences in background integration frequency between wild type and mutant lines were determined by one-way ANOVA with Dunnett's multiple comparisons test and are indicated with asterisks (* $p \leq 0.05$, ** $p \leq 0.01$, *** $p \leq 0.001$, **** $p \leq 0.0001$).

To determine the effect of DNA amount, 400 µl of 15 x 10^6 per ml cell suspension were electroporated with 2, 5, 10, 50 or 100 µg linearized pLPL DNA and diluted in different volumes (1, 1, 2.5, 5, 8 ml, respectively) of media to account for differences in background RI and produce approximately similar colony densities in unirradiated dishes; 150 µl aliquots of the diluted suspension were distributed into 8 PCR tubes, which were irradiated with 0–500 mGy and seeded into 10 cm dishes with 10 ml growth media; 5 µl and 50 µl aliquots were taken from the dishes irradiated with lowest and highest doses, seeded in triplicates into 6-well plates and used to estimate plating efficiency without selection and clonogenic survival. Colony numbers in 10 cm dishes after selection were adjusted for dilution and survival, and normalized to unirradiated control as in other experiments. Two independent experiments were performed.

bioRxiv preprint doi: https://doi.org/10.1101/614040; this version posted June 11, 2019. The copyright holder for this preprint (which was not certified by peer review) is the author/funder, who has granted bioRxiv a license to display the preprint in perpetuity. It is made available under aCC-BY-NC 4.0 International license.

For etoposide treatment, electroporated cells were seeded into 10 cm dishes containing a range of etoposide (Sigma E1383, stock solution 10 mM in DMSO) concentrations in 10 ml media; after seeding 5 µl and 50 µl aliquots were taken and plated in triplicate into 6-well plates containing 2 ml media with the same etoposide concentration; media was replaced next day and selection started in 10 cm dishes. Colony counts were adjusted for survival and normalized to untreated control. In the experiments involving kinase inhibitors, the stock solutions of chemicals (Ku-55933 10 mM in DMSO, VE-821 10 mM in DMSO, caffeine 40 mM in ES media, UCN-01 100 µM in DMSO, Wortmannin 1 mM in DMSO) were added to the media after seeding; 6 hr later media was collected and replaced with fresh media; collected media was centrifuged to pellet the cells, which were returned to the dish.

For FACS-based S-RI assays cells were electroporated with pEGFP-N1 or pAZ095, plated into 6 cm dishes at 3-6 x 10^5 per dish and irradiated. One or two days later the percentage of GFP-positive cells was determined (transient transfection efficiency). Upon reaching confluence cells were replated at 1:5-1:10 dilution into 6-well plates; this was repeated until 10-14 days after transfection at which point the percentage of GFP-positive cells (RI frequency) was measured.

Immunoblotting

Immunoblotting was performed following standard protocol by wet transfer to nitrocellulose or PVDF membrane, blocking and antibody dilution solution contained 5% dry skim milk, 0.05% Tween 20 in PBS. Secondary antibodies were either HRP-conjugated detected with ECL (GE), or fluorescent (Sigma, anti-mouse CF680 SAB4600199, anti-rabbit CF770 SAB4600215) detected with Odyssey CLx scanner (LiCOR). Primary antibodies: 53BP1 (Novus Biologicals, NB100-304), H2AX (Cell Signaling, #2595), γH2AX (pS139, Millipore JBW301), MDC1 ("exon8", Abcam, ab11171 and P2B11, Millipore, 05-1572), MCPH1 (Cell Signaling, #4120), Cyclin A (Santa Cruz, C-19), PARP-1 (ENZO, C-2-10).

Virus production

For rAAV production a confluent 10 cm dish of HEK293T cells was trypsinized and seeded at 1:2 dilution into a fresh 10 cm dish with 17 ml growth media. Calcium phosphate transfection was performed by mixing 10 µg each of the packaging (pHelper and pAAV-RC2) and 10 µg rAAV genome encoding GFP (pAAV-GFP) plasmids, 100 µl 2.5 M $CaCl_2$, deionised water to 1 ml; then 1 ml 2xHBS (16.4 g/l NaCl, 11.9 g/l HEPES, 0.21 g/l Na2HPO4; pH7.1 with NaOH) was added while bubbling air through the solution. The transfection mix was added dropwise to the cells. Media was changed next day and 10^6 HeLa cells were seeded for infection. Two days after transfection HEK293T cells were washed and dispersed with PBS containing 10 mM EDTA, pelleted, re-suspended in 1 ml media, frozen on dry ice/ethanol bath and thawed at 37 °C; the freeze-thaw cycle was performed the total of four times. Lysate was centrifuged at 10,000 rcf for 10 min. Half of the lysate was used to infect the HeLa cells. One day after infection HeLa cells were trypsinized and counted, divided over 10-15 10-cm dishes, which were irradiated with various doses. An aliquot was analyzed by FACS to determine the

bioRxiv preprint doi: https://doi.org/10.1101/614040; this version posted June 11, 2019. The copyright holder for this preprint (which was not certified by peer review) is the author/funder, who has granted bioRxiv a license to display the preprint in perpetuity. It is made available under aCC-BY-NC 4.0 International license.

transduction efficiency. On days 5-8 cells were checked and passaged if confluent. FACS analysis to determine the fraction of cells still expressing GFP was performed on days 8 to 13.

D64V mutation inactivating the integrase was introduced into lentiviral packaging plasmid pMDLg/pRRE by replacing the AgeI-AflII fragment with two overlapping PCR products, with mutation in the overlap, using Gibson assembly (pAZ139). HEK293T cells were transfected by calcium phosphate precipitation as described above with the third generation lentiviral packaging constructs pRSV-Rev, pMDLg/pRRE D64V (pAZ139) [84], and the plasmid encoding lentiviral genome with PGK-puroR (pLKO.1) alone or additionally with CMV-TurboGFP (SHC003, Sigma). Virus containing media was collected on days 2 and 3 after transfection, diluted 1:2 with the appropriate growth media and used to infect IB10 or HeLa cells (2x 10 cm-dishes). One day after the second infection the target cells were collected, pooled, distributed over three 145-mm dishes and irradiated with 0, 100, 400 mGy. Puromycin selection was started one day after irradiation.

Acknowledgements

We a thank Andre Nussenzweig and Frederick W. Alt for *H2ax*$^{-/-}$ lines, Francis Stewart, Hein te Riele, Titia Sixma and Alan Bradley for providing plasmid constructs, Gaëlle Legube for providing the AID-AsiSI-ER cell line, Yanto Ridwan for help with the micro-CT irradiations. This research was funded by the Gravitation program CancerGenomiCs.nl from the Netherlands Organization for Scientific Research (NWO) and is part of the Oncode Institute, which is partly financed by the Dutch Cancer Society. The research leading to these results has received funding from the European Atomic Energy Community's Seventh Framework Programme (FP7/2007-2011) under grant agreement n° 249689.

Author contributions

AZ and RK conceived and guided the study. AZ, MS, IB performed the experiments. AZ, MT, DvG, JE, RK supervised various parts of the study and participated in the interpretation of the results. AZ and RK wrote the manuscript, with contributions from other authors. All authors read and approved the manuscript.

Competing interests

Authors declare no competing interests.

bioRxiv preprint doi: https://doi.org/10.1101/614040; this version posted June 11, 2019. The copyright holder for this preprint (which was not certified by peer review) is the author/funder, who has granted bioRxiv a license to display the preprint in perpetuity. It is made available under aCC-BY-NC 4.0 International license.

Figures

Figure 1

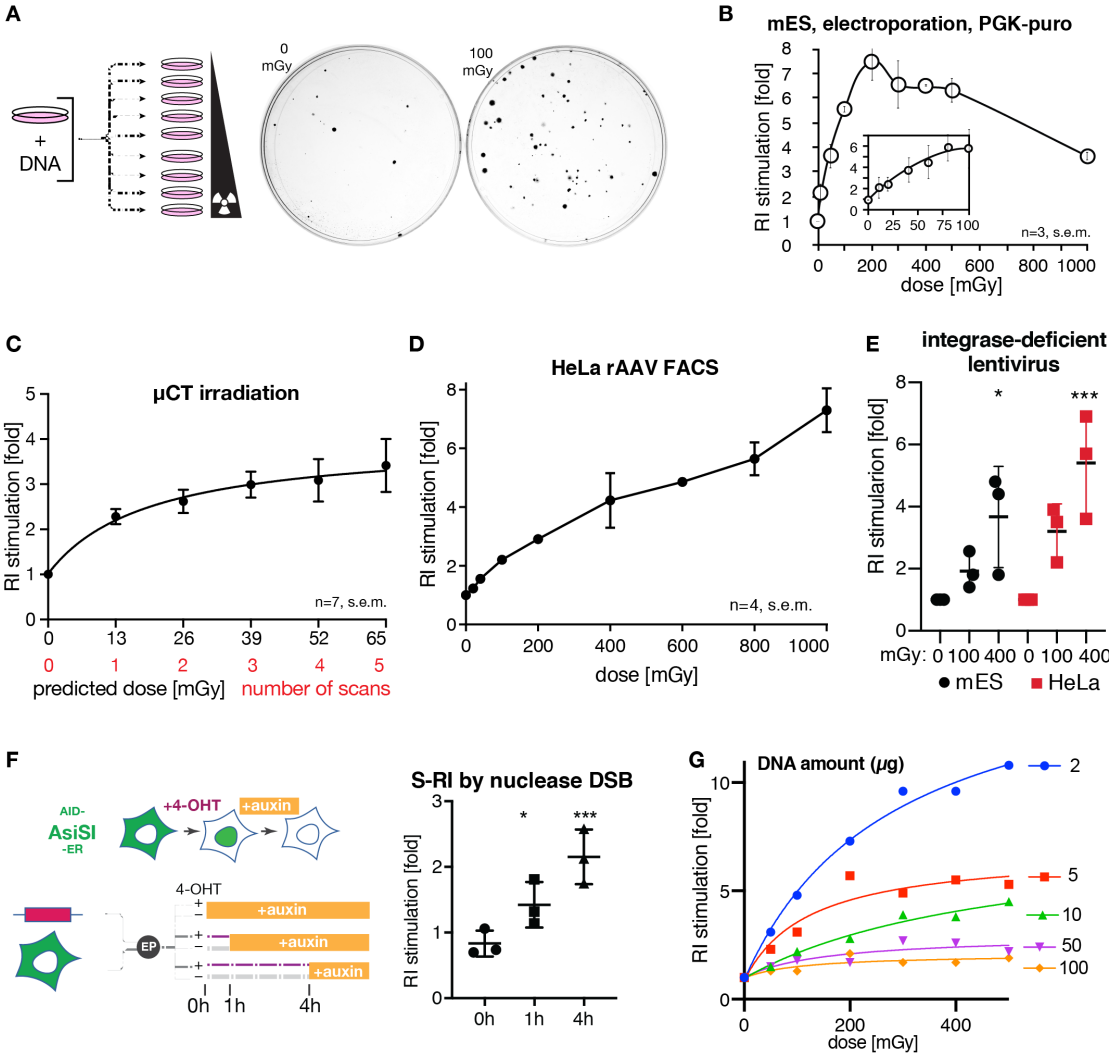

Figure 1 RI is strongly stimulated by low doses of ionizing radiation (**A**) Scheme of the typical S-RI assay, in which antibiotic-resistant colony formation is used as an end point. Cells are transfected with linear or circular plasmid DNA, divided over a series of dishes and irradiated with different doses. After 6-8 days of antibiotic selection, plates are stained and colonies counted. Representative examples of an unirradiated plate and a plate irradiated with 100 mGy are shown at the right. (**B**) Mouse ES cells were electroporated with linearized plasmid with puromycin resistance gene. Colony numbers were normalized to unirradiated control to give the fold increase in RI efficiency, which is plotted. (**C**) mES cells were electroporated with linear or circular pLPL plasmid, divided evenly into 6 vessels, and subjected to the indicated number of low resolution micro-CT scans in a Quantum FX instrument. Indicated doses are based on manufacturer's specification. n=7, error bars show s.e.m. (**D**) S-RI in HeLa cells infected with rAAV2-GFP and irradiated with the indicated doses one day later. Cells were maintained without selection, passaged when they reached confluency and sampled by FACS up to day 14. Representative FACS plots are shown in **[Fig S1C]**. The fraction of GFP positive cells in irradiated cultures normalized to unirradiated control is plotted. (**E**) S-RI in mES and HeLa cells infected with IDLV carrying puromycin-resistance gene and irradiated with the indicated doses. Ratio of colony numbers in irradiated to unirradiated plates determined in each experiment is plotted. Statistical significance indicated by asterisks was determined by ANOVA: * p≤0.05, *** p≤0.001. (**F**) S-RI by nuclease DSB. AID-AsiSI-ER U2OS cells containing a stably integrated coding sequence for AsiSI nuclease tagged with auxin-inducible degron (AID) and estrogen receptor (ER) domain that triggers re-localization from cytoplasm to the nucleus upon addition of tamoxifen (4-OHT). Cells were electroporated with linearized plasmid PGK-puro DNA and seeded immediately into dishes containing either 0 or 300 nM 4-OHT. Auxin was added at the indicated time points to induce AsiSI degradation. The ratio of puromycin resistant colony numbers formed in plates that contained 300 nM 4-OHT was divided by the number of colonies in 0 nM plates. Statistical significance indicated by asterisks was determined by ANOVA: * p≤0.05, *** p≤0.001. (**G**) Effect of the amount of transfected DNA on S-RI efficiency determined using colony-formation S-RI assay.

bioRxiv preprint doi: https://doi.org/10.1101/614040; this version posted June 11, 2019. The copyright holder for this preprint (which was not certified by peer review) is the author/funder, who has granted bioRxiv a license to display the preprint in perpetuity. It is made available under aCC-BY-NC 4.0 International license.

Supplementary Figure S1

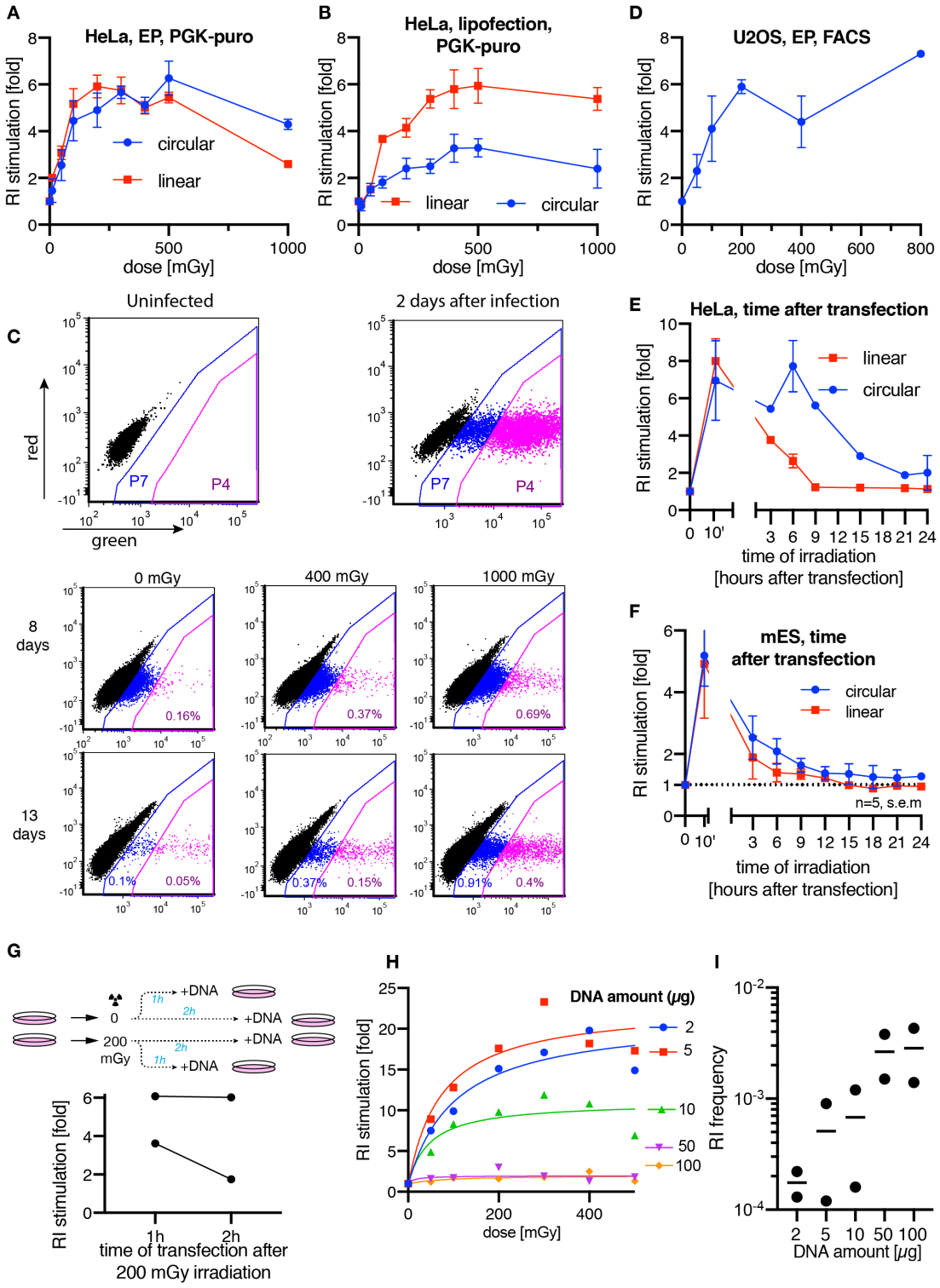

Figure S1 (related to Figure 1) (**A**) S-RI in HeLa cells transfected by electroporation with linear or circular plasmid DNA carrying puromycin resistance gene under a PGK promoter. (**B**) S-RI in HeLa cells transfected by lipofection. (**C**) Representative FACS plots from the rAAV S-RI experiments shown in **[Fig 1D]**. HeLa cells infected with rAAV2-GFP virus and analyzed at different time points after infection. Gates P4 and P7 were used to calculate the fraction of high GFP-positive and all GFP-positive cells, respectively. Percentage of GFP-positive cells drops precipitously from day 2 to day 8. At 8 days post infection the broader gate (P7) still contains cells that express GFP from transient infection, while the more stringent gate contains cells stably expressing GFP. (**D**) FACS-based S-RI assay performed with U2OS cells electroporated with the GFP-encoding plasmid DNA. (**E**) Stimulation of RI in HeLa cells electroporated with circular or linear plasmid DNA and irradiated with 0.2 Gy at different time points after electroporation. (**F**) Stimulation of RI in mES cells electroporated with circular or linear plasmid DNA and irradiated with 1 Gy at different time points after electroporation. Colony numbers were adjusted for reduced viability due to irradiation, and normalized to unirradiated control. (**G**) RI stimulation by irradiation of mES cells before transfection with linearized PGK-puro plasmid. Results of two independent experiments are plotted. (**H**) Repeat of the experiment shown in **[Fig 1G]**. (**I**) Background RI frequency (number of puromycin-resistant colonies per viable cell plated) from the experiments reported in **[Fig 1G, S1H]**.

bioRxiv preprint doi: https://doi.org/10.1101/614040; this version posted June 11, 2019. The copyright holder for this preprint (which was not certified by peer review) is the author/funder, who has granted bioRxiv a license to display the preprint in perpetuity. It is made available under aCC-BY-NC 4.0 International license.

Figure 2

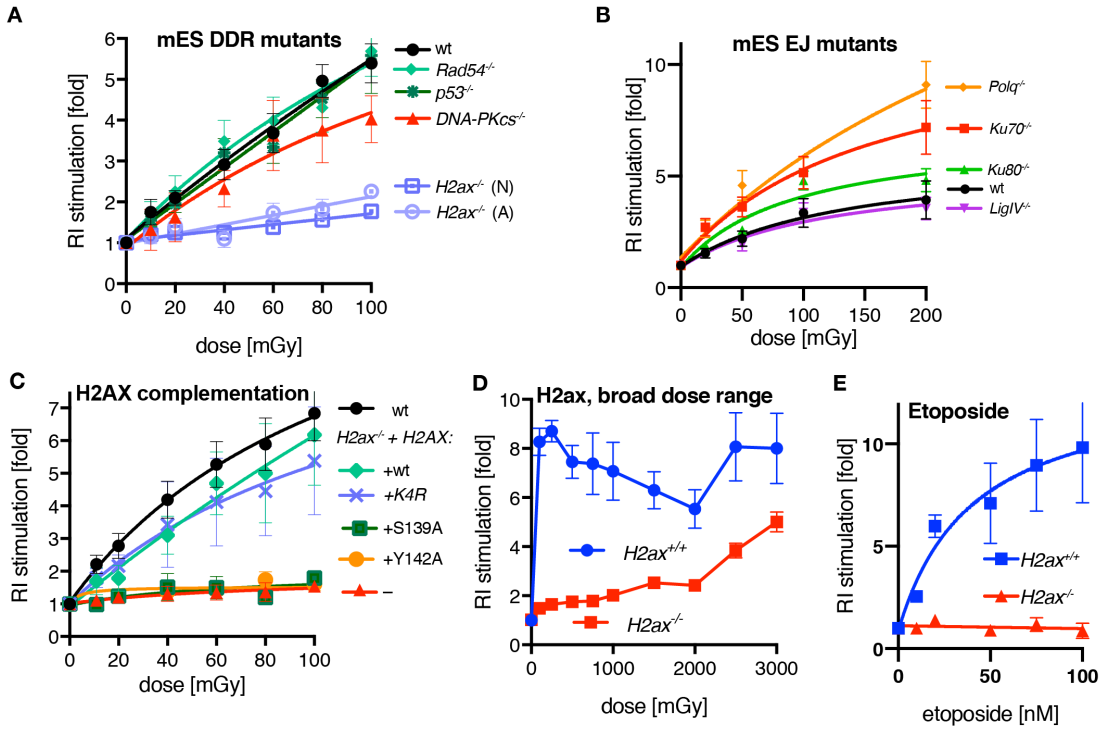

Figure 2 Genetic dependencies of the IR-stimulated random integration (**A**) Colony-based S-RI assay performed with mES cells deficient for key DSB repair and DNA damage response (DDR) proteins. The numbers of colonies obtained after puromycin selection were normalized to the unirradiated control. Means from at least 3 independent experiments, fitted with sigmoid curve, are plotted; error bars show s.e.m. (**B**) mES lines deficient for end joining proteins were assayed as in panel (A). (**C**) *H2ax*$^{-/-}$ (N) cells were complemented with versions of H2AX containing mutations in the residues involved in key post-translational modifications during the DNA damage response. A single copy of the respective *H2AX* genes was inserted in to the *Rosa26* locus. n=3, s.e.m. K4R designates a mutant in which four lysines subject to ubiquitination were replaced with arginines. (**D**) S-RI response to broad irradiation dose range of *H2ax*$^{-/-}$ and wild-type mES cells was measured in a colony-based S-RI assay. Each point represents means of at least six biological replicas, adjusted for reduced survival (**[Fig S2D]**), error bars indicated s.e.m. Both (N) and (A) *H2ax*$^{-/-}$ lines were used. (**E**) RI stimulation by etoposide measured by colony formation S-RI assay. Experiment was performed twice, with two independent *H2ax*$^{-/-}$ lines in each ((A) and (N)), data for each genotype was averaged, error bars indicate s.e.m.

bioRxiv preprint doi: https://doi.org/10.1101/614040; this version posted June 11, 2019. The copyright holder for this preprint (which was not certified by peer review) is the author/funder, who has granted bioRxiv a license to display the preprint in perpetuity. It is made available under aCC-BY-NC 4.0 International license.

Supplementary Figure S2

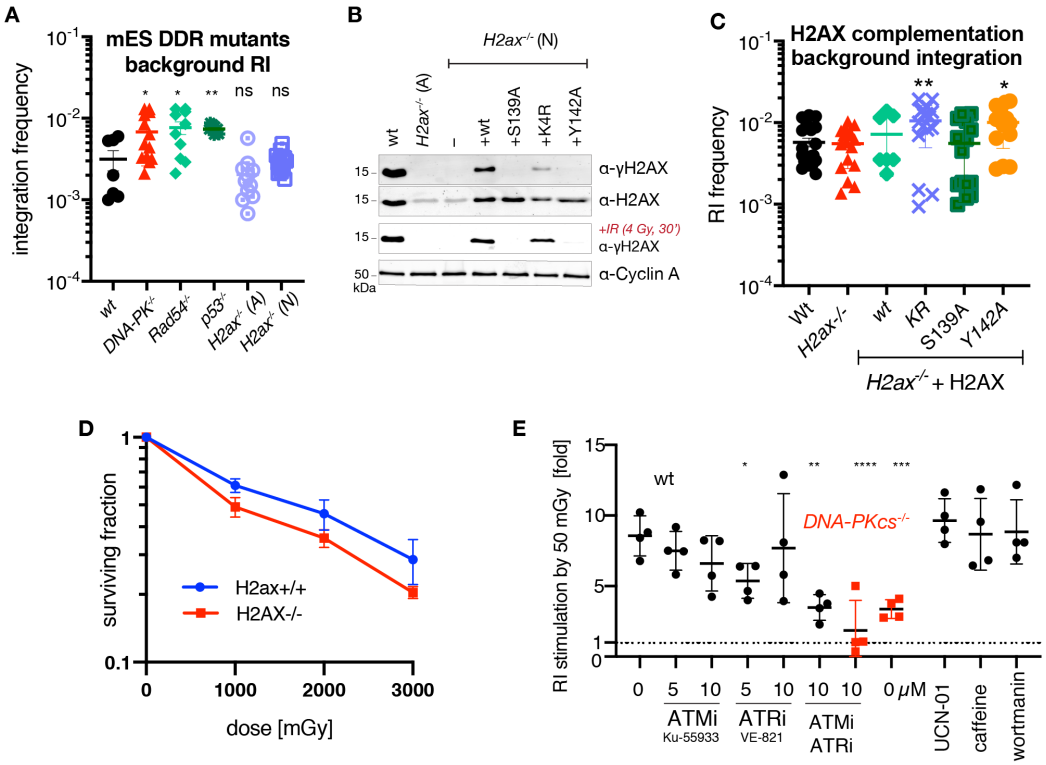

Figure S2 Genetic dependencies of stimulated random integration (related to Figure 2) (**A**) Background RI in the mutant cell lines used in S-RI assay from **[Fig 2A]**. Individual values from biological replicas are plotted, with bars indicating means ±s.e.m. Statistical significance was determined using one-way ANOVA with Dunnett's multiple comparison test. (**B**) Immunoblot of *H2ax*$^{-/-}$ and complemented lines. Total cell lysates from wild-type, *H2ax*$^{-/-}$ (A) and (N) lines, and *H2ax*$^{-/-}$ (N) line complemented with various H2AX mutants, were immunoblotted with the indicated antibodies. To test γH2AX induction cells were irradiated with 4 Gy and lysed 30 minutes after. (**C**) Background RI measured as in panel (A) in cells used in **[Fig 2C]**. (**D**) Samples from plates used in the S-RI assay plotted in **[Fig 2D]** were taken to determine the effect of irradiation on clonogenic survival of the wild-type and *H2ax*$^{-/-}$ cells to compensate for loss of viability in S-RI. (**E**) Effect of DNA damage response kinase inhibitors on S-RI in wild-type (black circles) and *DNA-PKcs*$^{-/-}$ (red squares) mES cells. Cells were electroporated with linearized plasmid, seeded into dishes containing the indicated concentrations of the inhibitors and irradiated with 50 mGy. The chemicals were removed 6 hours later. Data from four independent experiments is plotted.

bioRxiv preprint doi: https://doi.org/10.1101/614040; this version posted June 11, 2019. The copyright holder for this preprint (which was not certified by peer review) is the author/funder, who has granted bioRxiv a license to display the preprint in perpetuity. It is made available under aCC-BY-NC 4.0 International license.

Figure 3

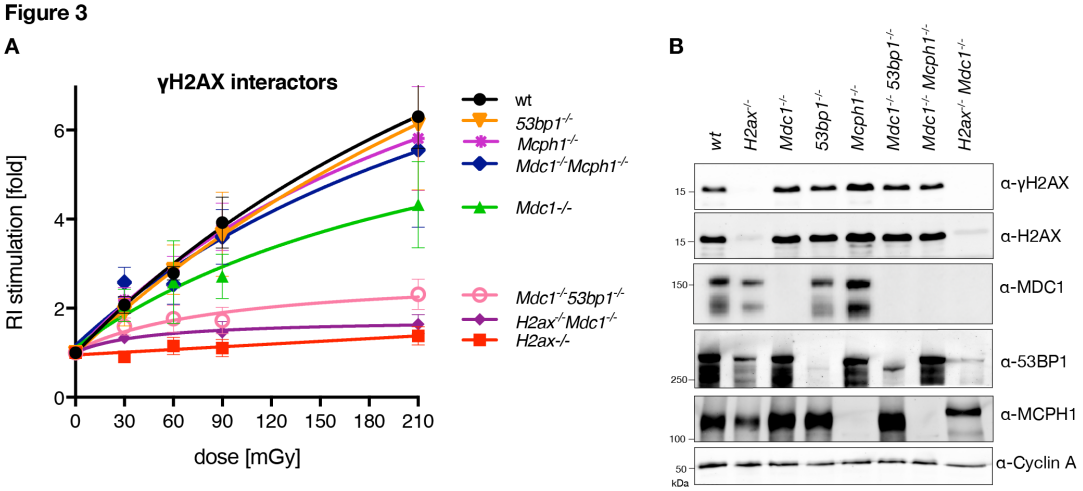

Figure 3 S-RI dependence on γH2AX-interacting proteins (**A**) Colony formation-based S-RI assay was performed on mES cells in which genes encoding the three known γH2AX-interacting proteins were inactivated by CRISPR/Cas9-assisted gene targeting. (**B**) Immunoblot on the whole cell lysates from the knock-out lines used in panel (A), confirming the loss of protein expression from targeted genes.

bioRxiv preprint doi: https://doi.org/10.1101/614040; this version posted June 11, 2019. The copyright holder for this preprint (which was not certified by peer review) is the author/funder, who has granted bioRxiv a license to display the preprint in perpetuity. It is made available under aCC-BY-NC 4.0 International license.

Supplmenetary Figure S3

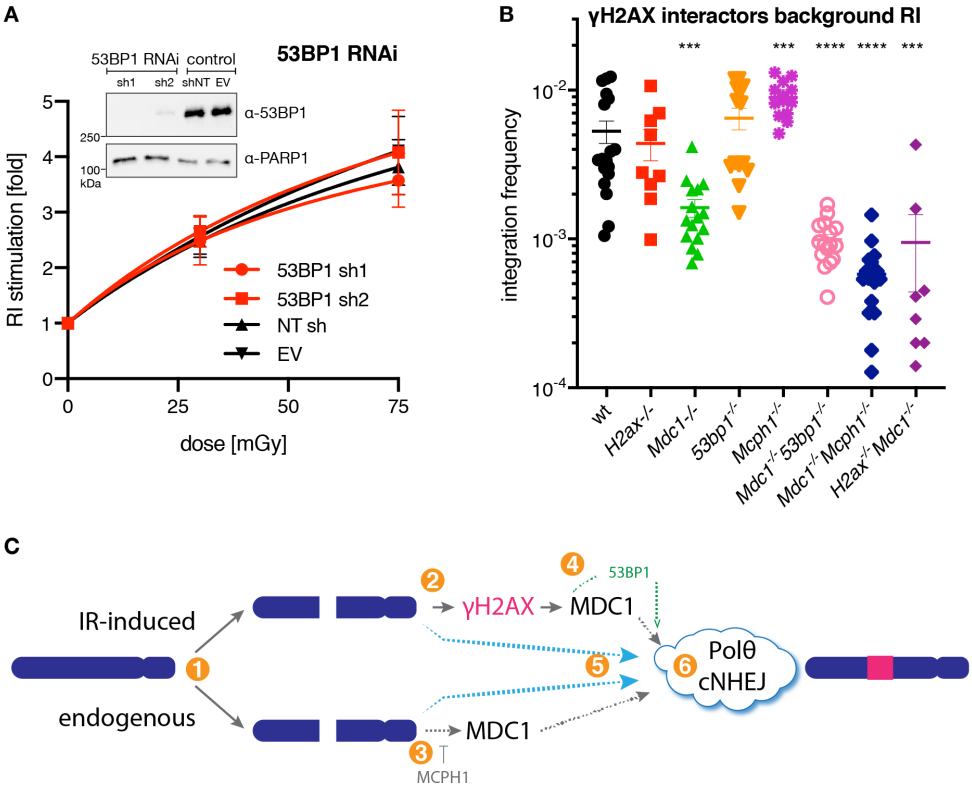

Figure S3 (related to Figure 3) (**A**) 53BP1 knock-down does not affect S-RI efficiency. Means of four independent puromycin-resistant colony formation S-RI assays (two with linearized, two with circular plasmid DNA) are plotted. Immunoblot on total cell lysates with the indicated antibodies confirming the efficiency of knock-down is shown as an inset. (**B**) Background RI efficiency in mES cell lines deficient for γH2AX interacting proteins. Data is plotted as in **[Fig S2A]**. (**C**) A model of RI and S-RI, based on the supposition that the initial stages of the two processes are mechanistically distinct 1, to account for the observation that S-RI is γH2AX-dependent 2, while RI is not 3; MCPH1 competes with MDC1 for γH2AX binding, and its removal results in elevated RI 3. MDC1 contributes to both RI and S-RI 4, and 53BP1 can provide a backup mechanism for S-RI in the absence of MDC1, but does not contribute to the RI process 4. Since neither RI nor S-RI are completely abolished by the deletion of the proteins listed in the scheme, alternative pathways must exist 5. The final ligation steps are mediated by Pol θ or cNHEJ 6, as we previously showed that all integration events in ES cells are abolished when both these end joining mechanisms are inactivated, however the relative contribution of Pol θ and cNHEJ to RI and S-RI may be different.

bioRxiv preprint doi: https://doi.org/10.1101/614040; this version posted June 11, 2019. The copyright holder for this preprint (which was not certified by peer review) is the author/funder, who has granted bioRxiv a license to display the preprint in perpetuity. It is made available under aCC-BY-NC 4.0 International license.

Supplementary Figure S4

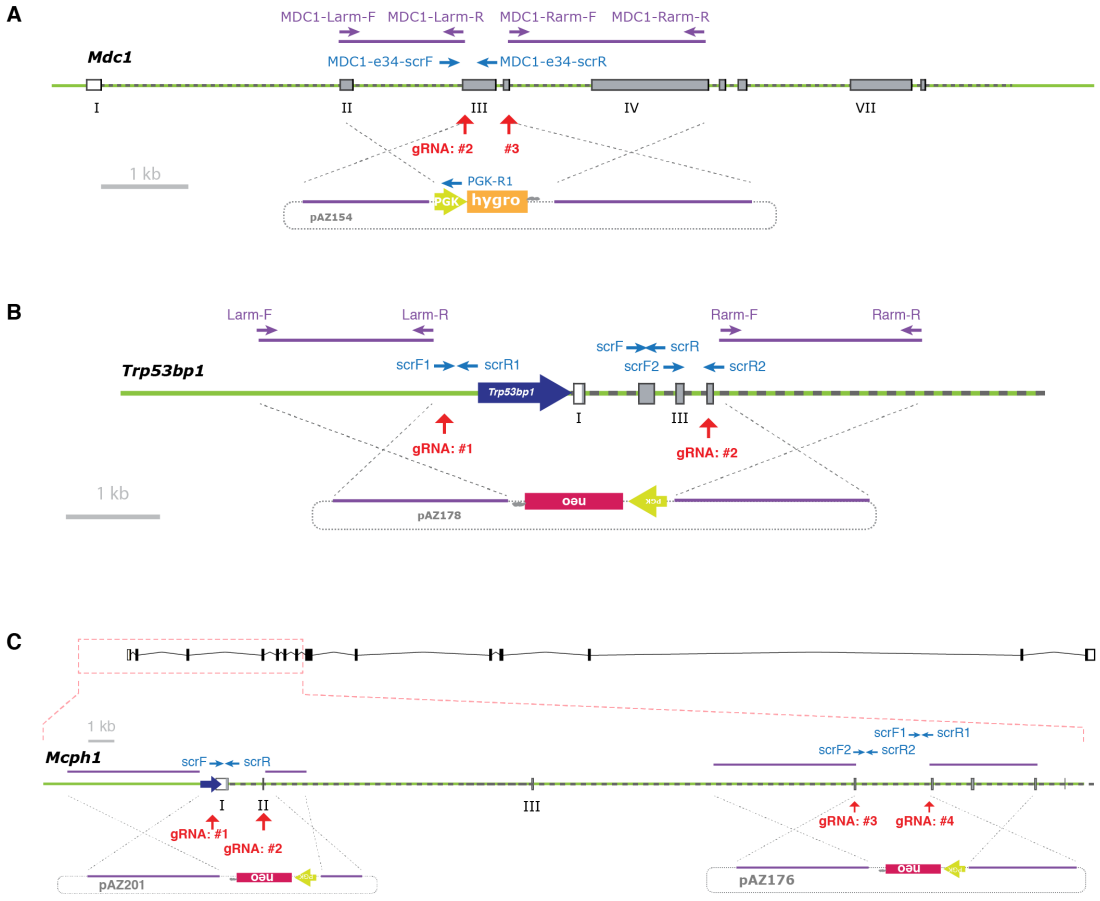

Figure S4 Generation of knock-out mES lines by CRISPR/Cas9-assisted gene targeting Schemes of mouse loci (**A**) *Mdc1,* (**B**) *53bp1* and (**C**) *Mcph1* and of the corresponding gene targeting construct are shown. CRISPR/Cas9 cut sites (gRNA recognition sequences) are indicated with red arrows. Homology arms and PCR primers used to amplify them from genomic DNA for cloning into the gene targeting construct are shown as violet bars and arrows, respectively. Locations of the PCR primers used to screen for homozygously targeted clones are shown as blue arrows. Endogenous and synthetic promotors are shown as thick arrows. Exons and antibiotic resistance genes are shown as bars.

bioRxiv preprint doi: https://doi.org/10.1101/614040; this version posted June 11, 2019. The copyright holder for this preprint (which was not certified by peer review) is the author/funder, who has granted bioRxiv a license to display the preprint in perpetuity. It is made available under aCC-BY-NC 4.0 International license.

Supplementary Figure S5

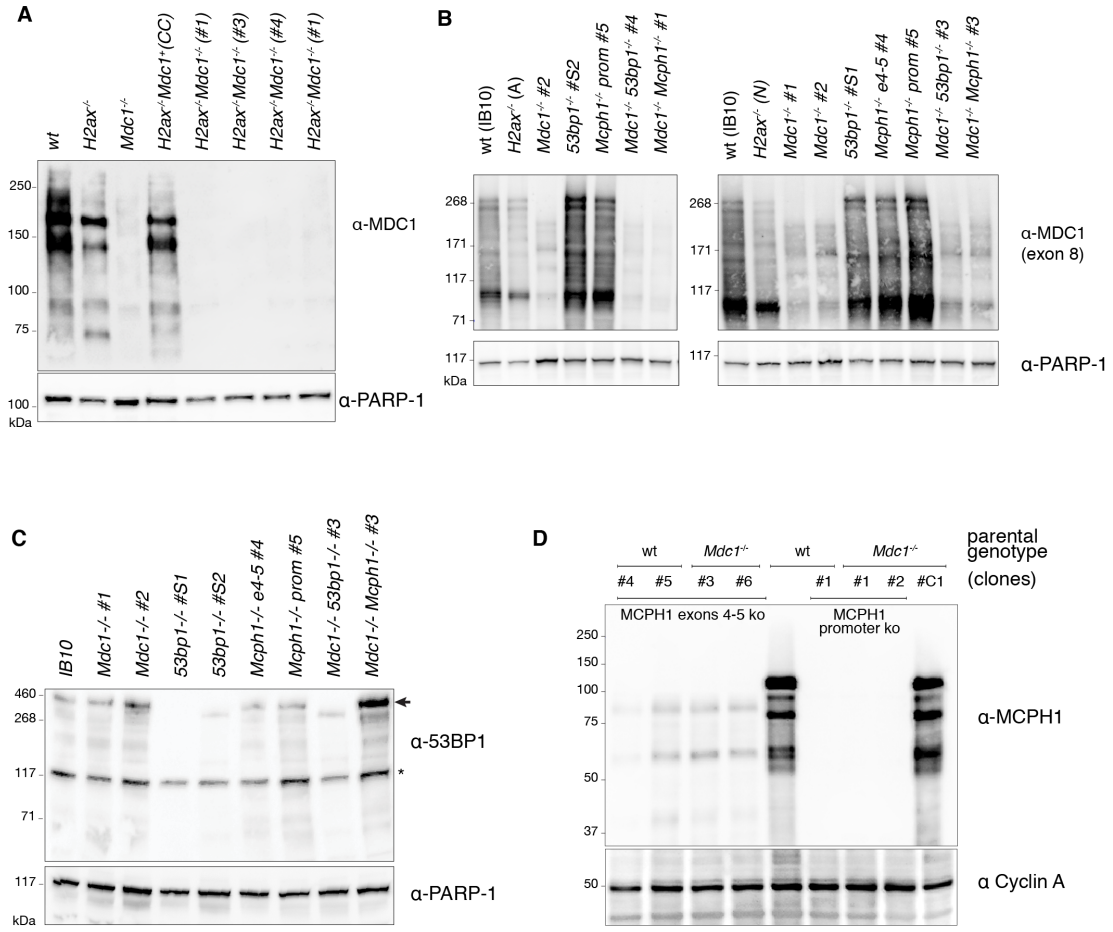

Figure S5 Immunoblots confirming the loss of protein expression from targeted genes Total cell extracts from the mES cell lines with indicated genotypes were fractionated by SDS-PAGE and immunoblotted with the indicated antibodies: (**A**) anti-MDC1 monoclonal and (**B**) polyclonal raised against the region encoded by exon 8, (**C**) anti-53BP1 and (**D**) anti-MCPH1. Membranes were re-probed with anti-PARP-1 antibody to assess relative loading. For each genotype at least two independent clones used in the experiments were tested. Clones that were derived from the CRISPR/Cas9-assisted gene targeting procedure but retained the wild-type allele (as determined by PCR genotyping) were used as controls in some experiments; these are indicated with letter C. Asterisk indicates non-specific band.

bioRxiv preprint doi: https://doi.org/10.1101/614040; this version posted June 11, 2019. The copyright holder for this preprint (which was not certified by peer review) is the author/funder, who has granted bioRxiv a license to display the preprint in perpetuity. It is made available under aCC-BY-NC 4.0 International license.

References

1. Uren AG, Kool J, Berns A, van Lohuizen M. Retroviral insertional mutagenesis: past, present and future. Oncogene. Nature Publishing Group; 2005;24: 7656–7672. doi:10.1038/sj.onc.1209043

2. Chen Y, Williams V, Filippova M, Filippov V, Duerksen-Hughes P. Viral Carcinogenesis: Factors Inducing DNA Damage and Virus Integration. Cancers. Multidisciplinary Digital Publishing Institute; 2014;6: 2155–2186. doi:10.3390/cancers6042155

3. Capecchi MR. Altering the genome by homologous recombination. Science. 1989;244: 1288–1292.

4. Nabetani A, Ishikawa F. Unusual telomeric DNAs in human telomerase-negative immortalized cells. Mol Cell Biol. 2009;29: 703–713. doi:10.1128/MCB.00603-08

5. Schnepp BC, Jensen RL, Chen C-L, Johnson PR, Clark KR. Characterization of adeno-associated virus genomes isolated from human tissues. J Virol. American Society for Microbiology; 2005;79: 14793–14803. doi:10.1128/JVI.79.23.14793-14803.2005

6. Bergsmedh A, Szeles A, Henriksson M, Bratt A, Folkman MJ, Spetz AL, et al. Horizontal transfer of oncogenes by uptake of apoptotic bodies. Proc Natl Acad Sci USA. 2001;98: 6407–6411. doi:10.1073/pnas.101129998

7. Shibata Y, Kumar P, Layer R, Willcox S, Gagan JR, Griffith JD, et al. Extrachromosomal microDNAs and chromosomal microdeletions in normal tissues. Science. 2012;336: 82–86. doi:10.1126/science.1213307

8. Würtele H, Little KCE, Chartrand P. Illegitimate DNA integration in mammalian cells. Gene Ther. Nature Publishing Group; 2003;10: 1791–1799. doi:10.1038/sj.gt.3302074

9. Kamekawa H, Kurosawa A, Umehara M, Toyoda E, Adachi N. Endogenous Factors Causative of Spontaneous DNA Damage that Leads to Random Integration in Human Cells. Gene Technology. 2013;02: 1–5. doi:10.4172/2329-6682.1000105

10. Hillman GG, Xu M, Wang Y, Wright JL, Lu X, Kallinteris NL, et al. Radiation improves intratumoral gene therapy for induction of cancer vaccine in murine prostate carcinoma. Hum Gene Ther. 2003;14: 763–775. doi:10.1089/104303403765255156

11. Kiechle M, Manivasakam P, Eckardt-Schupp F, Schiestl RH, Friedl AA. Promoter-trapping in Saccharomyces cerevisiae by radiation-assisted fragment insertion. Nucleic Acids Res. 2002;30: e136.

12. Stevens CW, Puppi M, Cerniglia GJ. Time-dose relationships in radiation-enhanced integration. Int J Radiat Biol. 2001;77: 841–846. doi:10.1080/09553000110053882

13. Zeng M, Cerniglia GJ, Eck SL, Stevens CW. High-efficiency stable gene transfer of adenovirus into mammalian cells using ionizing radiation. Hum Gene Ther. 1997;8: 1025–1032. doi:10.1089/hum.1997.8.9-1025

14. Iwamoto R, Fushimi K, Hiraki Y, Namba M. Enhancement of DNA-transfection frequency by X-rays. Acta Med Okayama. 1997;51: 19–23.

bioRxiv preprint doi: https://doi.org/10.1101/614040; this version posted June 11, 2019. The copyright holder for this preprint (which was not certified by peer review) is the author/funder, who has granted bioRxiv a license to display the preprint in perpetuity. It is made available under aCC-BY-NC 4.0 International license.

15. Stevens CW, Zeng M, Cerniglia GJ. Ionizing radiation greatly improves gene transfer efficiency in mammalian cells. Hum Gene Ther. 1996;7: 1727–1734. doi:10.1089/hum.1996.7.14-1727

16. Alexander IE, Russell DW, Miller AD. DNA-damaging agents greatly increase the transduction of nondividing cells by adeno-associated virus vectors. J Virol. 1994;68: 8282–8287.

17. Rubin JS. Effect of gamma rays on efficiency of gene transfer in DNA repair-proficient and -deficient cell lines. Somat Cell Mol Genet. 1988;14: 613–621.

18. Perez CF, Botchan MR, Tobias CA. DNA-mediated gene transfer efficiency is enhanced by ionizing and ultraviolet irradiation of rodent cells in vitro. I. Kinetics of enhancement. Radiat Res. 1985;104: 200–213.

19. Debenham PG, Webb MB. The effect of X-rays and ultraviolet light on DNA-mediated gene transfer in mammalian cells. Int J Radiat Biol Relat Stud Phys Chem Med. 1984;46: 555–568.

20. Yang TC, Tobias CA, Blakely EA, Craise LM, Madfes IS, Perez C, et al. Enhancement effects of high-energy neon particles on the viral transformation of mouse C3H1OT1/2 cells in vitro. Radiat Res. 1980;81: 208–223.

21. Coggin JH. Enhanced virus transformation of hamster embryo cells in vitro. J Virol. American Society for Microbiology (ASM); 1969;3: 458–462.

22. Pollock EJ, Todaro GJ. Radiation enhancement of SV40 transformation in 3T3 and human cells. Nature. 1968;219: 520–521.

23. Stoker M. EFFECT OF X-IRRADIATION ON SUSCEPTIBILITY OF CELLS TO TRANSFORMATION BY POLYOMA VIRUS. Nature. 1963;200: 756–758.

24. Lin EC. Radiation risk from medical imaging. Mayo Clin Proc. 2010;85: 1142–6– quiz 1146. doi:10.4065/mcp.2010.0260

25. Kaeppel C, Beattie SG, Fronza R, van Logtenstein R, Salmon F, Schmidt S, et al. A largely random AAV integration profile after LPLD gene therapy. Nat Med. 2013;19: 889–891. doi:10.1038/nm.3230

26. Miller DG, Petek LM, Russell DW. Adeno-associated virus vectors integrate at chromosome breakage sites. Nat Genet. 2004;36: 767–773. doi:10.1038/ng1380

27. Yáñez-Muñoz RJ, Balaggan KS, MacNeil A, Howe SJ, Schmidt M, Smith AJ, et al. Effective gene therapy with nonintegrating lentiviral vectors. Nat Med. 2006;12: 348–353. doi:10.1038/nm1365

28. Vargas J, Gusella GL, Najfeld V, Klotman ME, Cara A. Novel integrase-defective lentiviral episomal vectors for gene transfer. Hum Gene Ther. 2004;15: 361–372. doi:10.1089/104303404322959515

29. Leavitt AD, Robles G, Alesandro N, Varmus HE. Human immunodeficiency virus type 1 integrase mutants retain in vitro integrase activity yet fail to integrate viral DNA efficiently during infection. J Virol. 1996;70: 721–728.

30. Wang X, Wang Y, Wu X, Wang J, Wang Y, Qiu Z, et al. Unbiased detection of off-target cleavage by CRISPR-Cas9 and TALENs using integrase-defective lentiviral vectors. Nat Biotechnol. 2015;33: 175–178. doi:10.1038/nbt.3127

bioRxiv preprint doi: https://doi.org/10.1101/614040; this version posted June 11, 2019. The copyright holder for this preprint (which was not certified by peer review) is the author/funder, who has granted bioRxiv a license to display the preprint in perpetuity. It is made available under aCC-BY-NC 4.0 International license.

31. Gabriel R, Lombardo A, Arens A, Miller JC, Genovese P, Kaeppel C, et al. An unbiased genome-wide analysis of zinc-finger nuclease specificity. Nat Biotechnol. 2011;29: 816–823. doi:10.1038/nbt.1948

32. Aymard F, Bugler B, Schmidt CK, Guillou E, Caron P, Briois S, et al. Transcriptionally active chromatin recruits homologous recombination at DNA double-strand breaks. Nature Structural and Molecular Biology. 2014;21: 366–374. doi:10.1038/nsmb.2796

33. Essers J, Hendriks RW, Swagemakers SM, Troelstra C, de Wit J, Bootsma D, et al. Disruption of mouse RAD54 reduces ionizing radiation resistance and homologous recombination. Cell. 1997;89: 195–204.

34. Gao Y, Chaudhuri J, Zhu C, Davidson L, Weaver DT, Alt FW. A targeted DNA-PKcs-null mutation reveals DNA-PK-independent functions for KU in V(D)J recombination. Immunity. 1998;9: 367–376.

35. Zelensky AN, Schimmel J, Kool H, Kanaar R, Tijsterman M. Inactivation of Pol θ and C-NHEJ eliminates off-target integration of exogenous DNA. Nat Commun. Nature Publishing Group; 2017;8: 66. doi:10.1038/s41467-017-00124-3

36. Saito S, Maeda R, Adachi N. Dual loss of human POLQ and LIG4 abolishes random integration. Nat Commun. 2017;8: 16112. doi:10.1038/ncomms16112

37. Bassing CH, Chua KF, Sekiguchi J, Suh H, Whitlow SR, Fleming JC, et al. Increased ionizing radiation sensitivity and genomic instability in the absence of histone H2AX. Proc Natl Acad Sci USA. National Academy of Sciences; 2002;99: 8173–8178. doi:10.1073/pnas.122228699

38. Celeste A, Petersen S, Romanienko PJ, Fernandez-Capetillo O, Chen HT, Sedelnikova OA, et al. Genomic instability in mice lacking histone H2AX. Science. 2002;296: 922–927. doi:10.1126/science.1069398

39. Bassing CH, Suh H, Ferguson DO, Chua KF, Manis J, Eckersdorff M, et al. Histone H2AX: a dosage-dependent suppressor of oncogenic translocations and tumors. Cell. 2003;114: 359–370.

40. Franco S, Gostissa M, Zha S, Lombard DB, Murphy MM, Zarrin AA, et al. H2AX prevents DNA breaks from progressing to chromosome breaks and translocations. Mol Cell. 2006;21: 201–214. doi:10.1016/j.molcel.2006.01.005

41. Rogakou EP, Pilch DR, Orr AH, Ivanova VS, Bonner WM. DNA double-stranded breaks induce histone H2AX phosphorylation on serine 139. Journal of Biological Chemistry. 1998;273: 5858–5868.

42. Stewart GS, Panier S, Townsend K, Al-Hakim AK, Kolas NK, Miller ES, et al. The RIDDLE syndrome protein mediates a ubiquitin-dependent signaling cascade at sites of DNA damage. Cell. 2009;136: 420–434. doi:10.1016/j.cell.2008.12.042

43. Mattiroli F, Vissers JHA, van Dijk WJ, Ikpa P, Citterio E, Vermeulen W, et al. RNF168 ubiquitinates K13-15 on H2A/H2AX to drive DNA damage signaling. Cell. 2012;150: 1182–1195. doi:10.1016/j.cell.2012.08.005

44. Stucki M, Clapperton JA, Mohammad D, Yaffe MB, Smerdon SJ, Jackson SP. MDC1 directly binds phosphorylated histone H2AX to regulate cellular responses to DNA double-strand breaks. Cell. 2005;123: 1213–1226. doi:10.1016/j.cell.2005.09.038

bioRxiv preprint doi: https://doi.org/10.1101/614040; this version posted June 11, 2019. The copyright holder for this preprint (which was not certified by peer review) is the author/funder, who has granted bioRxiv a license to display the preprint in perpetuity. It is made available under aCC-BY-NC 4.0 International license.

45. Toyoda E, Kurosawa A, Kamekawa H, Adachi N. Topoisomerase IIalpha inhibition following DNA transfection greatly enhances random integration in a human pre-B lymphocyte cell line. Biochem Biophys Res Commun. 2009;382: 492–496. doi:10.1016/j.bbrc.2009.03.047

46. Aratani Y, Andoh T, Koyama H. Effects of DNA topoisomerase inhibitors on nonhomologous and homologous recombination in mammalian cells. Mutat Res. 1996;362: 181–191.

47. Bodley AL, Huang HC, Yu C, Liu LF. Integration of simian virus 40 into cellular DNA occurs at or near topoisomerase II cleavage hot spots induced by VM-26 (teniposide). Mol Cell Biol. 1993;13: 6190–6200.

48. Stiff T, O'Driscoll M, Rief N, Iwabuchi K, Löbrich M, Jeggo PA. ATM and DNA-PK function redundantly to phosphorylate H2AX after exposure to ionizing radiation. Cancer Res. 2004;64: 2390–2396.

49. Hickson I, Zhao Y, Richardson CJ, Green SJ, Martin NMB, Orr AI, et al. Identification and characterization of a novel and specific inhibitor of the ataxia-telangiectasia mutated kinase ATM. Cancer Res. 2004;64: 9152–9159. doi:10.1158/0008-5472.CAN-04-2727

50. Charrier J-D, Durrant SJ, Golec JMC, Kay DP, Knegtel RMA, MacCormick S, et al. Discovery of potent and selective inhibitors of ataxia telangiectasia mutated and Rad3 related (ATR) protein kinase as potential anticancer agents. J Med Chem. 2011;54: 2320–2330. doi:10.1021/jm101488z

51. Sarkaria JN, Tibbetts RS, Busby EC, Kennedy AP, Hill DE, Abraham RT. Inhibition of phosphoinositide 3-kinase related kinases by the radiosensitizing agent wortmannin. Cancer Res. 1998;58: 4375–4382.

52. Graves PR, Yu L, Schwarz JK, Gales J, Sausville EA, O'Connor PM, et al. The Chk1 protein kinase and the Cdc25C regulatory pathways are targets of the anticancer agent UCN-01. Journal of Biological Chemistry. 2000;275: 5600–5605.

53. Zelensky AN, Sanchez H, Ristic D, Vidic I, van Rossum-Fikkert SE, Essers J, et al. Caffeine suppresses homologous recombination through interference with RAD51-mediated joint molecule formation. Nucleic Acids Res. 2013;41: 6475–6489. doi:10.1093/nar/gkt375

54. Tsabar M, Mason JM, Chan Y-L, Bishop DK, Haber JE. Caffeine inhibits gene conversion by displacing Rad51 from ssDNA. Nucleic Acids Res. 2015;43: 6902–6918. doi:10.1093/nar/gkv525

55. Tsabar M, Eapen VV, Mason JM, Memisoglu G, Waterman DP, Long MJ, et al. Caffeine impairs resection during DNA break repair by reducing the levels of nucleases Sae2 and Dna2. Nucleic Acids Res. 2015;43: 6889–6901. doi:10.1093/nar/gkv520

56. Kleiner RE, Verma P, Molloy KR, Chait BT, Kapoor TM. Chemical proteomics reveals a γH2AX-53BP1 interaction in the DNA damage response. Nat Chem Biol. Nature Publishing Group; 2015;11: 807–814. doi:10.1038/nchembio.1908

57. Wood JL, Singh N, Mer G, Chen J. MCPH1 functions in an H2AX-dependent but MDC1-independent pathway in response to DNA damage. Journal of Biological Chemistry. 2007;282: 35416–35423. doi:10.1074/jbc.M705245200

58. Scully R, Xie A. Double strand break repair functions of histone H2AX. Mutat Res. 2013;750: 5–14. doi:10.1016/j.mrfmmm.2013.07.007

bioRxiv preprint doi: https://doi.org/10.1101/614040; this version posted June 11, 2019. The copyright holder for this preprint (which was not certified by peer review) is the author/funder, who has granted bioRxiv a license to display the preprint in perpetuity. It is made available under aCC-BY-NC 4.0 International license.

59. Chen W-T, Alpert A, Leiter C, Gong F, Jackson SP, Miller KM. Systematic identification of functional residues in mammalian histone H2AX. Mol Cell Biol. 2013;33: 111–126. doi:10.1128/MCB.01024-12

60. Revet I, Feeney L, Bruguera S, Wilson W, Dong TK, Oh DH, et al. Functional relevance of the histone gammaH2Ax in the response to DNA damaging agents. Proc Natl Acad Sci USA. National Academy of Sciences; 2011;108: 8663–8667. doi:10.1073/pnas.1105866108

61. Sonoda E, Zhao GY, Kohzaki M, Dhar PK, Kikuchi K, Redon C, et al. Collaborative roles of gammaH2AX and the Rad51 paralog Xrcc3 in homologous recombinational repair. DNA Repair (Amst). 2007;6: 280–292. doi:10.1016/j.dnarep.2006.10.025

62. Celeste A, Fernandez-Capetillo O, Kruhlak MJ, Pilch DR, Staudt DW, Lee A, et al. Histone H2AX phosphorylation is dispensable for the initial recognition of DNA breaks. Nat Cell Biol. Nature Publishing Group; 2003;5: 675–679. doi:10.1038/ncb1004

63. Xie A, Puget N, Shim I, Odate S, Jarzyna I, Bassing CH, et al. Control of sister chromatid recombination by histone H2AX. Mol Cell. 2004;16: 1017–1025. doi:10.1016/j.molcel.2004.12.007

64. Xie A, Odate S, Chandramouly G, Scully R. H2AX post-translational modifications in the ionizing radiation response and homologous recombination. Cell Cycle. 2010;9: 3602–3610. doi:10.4161/cc.9.17.12884

65. Fernandez-Capetillo O, Chen HT, Celeste A, Ward I, Romanienko PJ, Morales JC, et al. DNA damage-induced G2-M checkpoint activation by histone H2AX and 53BP1. Nat Cell Biol. Nature Publishing Group; 2002;4: 993–997. doi:10.1038/ncb884

66. Xie A, Kwok A, Scully R. Role of mammalian Mre11 in classical and alternative nonhomologous end joining. Nature Structural and Molecular Biology. 2009;16: 814–818. doi:10.1038/nsmb.1640

67. Bañuelos CA, Banáth JP, MacPhail SH, Zhao J, Eaves CA, O'Connor MD, et al. Mouse but not human embryonic stem cells are deficient in rejoining of ionizing radiation-induced DNA double-strand breaks. DNA Repair (Amst). 2008;7: 1471–1483. doi:10.1016/j.dnarep.2008.05.005

68. Panier S, Boulton SJ. Double-strand break repair: 53BP1 comes into focus. Nat Rev Mol Cell Biol. Nature Publishing Group; 2014;15: 7–18. doi:10.1038/nrm3719

69. Zimmermann M, de Lange T. 53BP1: pro choice in DNA repair. Trends Cell Biol. 2014;24: 108–117. doi:10.1016/j.tcb.2013.09.003

70. Bunting SF, Callén E, Wong N, Chen HT, Polato F, Gunn A, et al. 53BP1 inhibits homologous recombination in Brca1-deficient cells by blocking resection of DNA breaks. Cell. 2010;141: 243–254. doi:10.1016/j.cell.2010.03.012

71. Difilippantonio S, Gapud E, Wong N, Huang C-Y, Mahowald G, Chen HT, et al. 53BP1 facilitates long-range DNA end-joining during V(D)J recombination. Nature. Nature Publishing Group; 2008;456: 529–533. doi:10.1038/nature07476

72. Dimitrova N, Chen Y-CM, Spector DL, de Lange T. 53BP1 promotes non-homologous end joining of telomeres by increasing chromatin mobility. Nature. 2008;456: 524–528. doi:10.1038/nature07433

73. Lou Z, Chen BP-C, Asaithamby A, Minter-Dykhouse K, Chen DJ, Chen J. MDC1 regulates DNA-PK autophosphorylation in response to DNA damage. Journal of Biological Chemistry.

bioRxiv preprint doi: https://doi.org/10.1101/614040; this version posted June 11, 2019. The copyright holder for this preprint (which was not certified by peer review) is the author/funder, who has granted bioRxiv a license to display the preprint in perpetuity. It is made available under aCC-BY-NC 4.0 International license.

American Society for Biochemistry and Molecular Biology; 2004;279: 46359–46362. doi:10.1074/jbc.C400375200

74. Stewart GS, Wang B, Bignell CR, Taylor AMR, Elledge SJ. MDC1 is a mediator of the mammalian DNA damage checkpoint. Nature. 2003;421: 961–966. doi:10.1038/nature01446

75. Minter-Dykhouse K, Ward I, Huen MSY, Chen J, Lou Z. Distinct versus overlapping functions of MDC1 and 53BP1 in DNA damage response and tumorigenesis. J Cell Biol. 2008;181: 727–735. doi:10.1083/jcb.200801083

76. Eliezer Y, Argaman L, Rhie A, Doherty AJ, Goldberg M. The direct interaction between 53BP1 and MDC1 is required for the recruitment of 53BP1 to sites of damage. Journal of Biological Chemistry. American Society for Biochemistry and Molecular Biology; 2009;284: 426–435. doi:10.1074/jbc.M807375200

77. Hooper M, Hardy K, Handyside A, Hunter S, Monk M. HPRT-deficient (Lesch-Nyhan) mouse embryos derived from germline colonization by cultured cells. Nature. 1987;326: 292–295. doi:10.1038/326292a0

78. Ran FA, Hsu PD, Wright J, Agarwala V, Scott DA, Zhang F. Genome engineering using the CRISPR-Cas9 system. Nat Protoc. Nature Publishing Group; 2013;8: 2281–2308. doi:10.1038/nprot.2013.143

79. Soriano P. Generalized lacZ expression with the ROSA26 Cre reporter strain. Nat Genet. 1999;21: 70–71. doi:10.1038/5007

80. Dannenberg J-H, Schuijff L, Dekker M, van der Valk M, Riele Te H. Tissue-specific tumor suppressor activity of retinoblastoma gene homologs p107 and p130. Genes Dev. Cold Spring Harbor Lab; 2004;18: 2952–2962. doi:10.1101/gad.322004

81. Li MZ, Elledge SJ. SLIC: a method for sequence- and ligation-independent cloning. Methods Mol Biol. 2012;852: 51–59. doi:10.1007/978-1-61779-564-0_5

82. Gibson DG, Young L, Chuang R-Y, Venter JC, Hutchison CA, Smith HO. Enzymatic assembly of DNA molecules up to several hundred kilobases. Nat Meth. 2009;6: 343–345. doi:10.1038/nmeth.1318

83. Fu J, Anastassiadis K, Stewart AF. A recombineering pipeline to make conditional targeting constructs. Meth Enzymol. 2010;477: 125–144. doi:10.1016/S0076-6879(10)77008-7

84. Dull T, Zufferey R, Kelly M, Mandel RJ, Nguyen M, Trono D, et al. A third-generation lentivirus vector with a conditional packaging system. J Virol. 1998;72: 8463–8471.